The influence of stearic acid coating on the properties of magnesium hydroxide, hydromagnesite and hydrotalcite powders

Walter W Focke[1,*], Dan Molefe[2], FJW Labuschagne[1] and Shatish Ramjee[1]

Institute of Applied Materials, Department of Chemical Engineering[1] and Department of Chemistry[2], University of Pretoria, Lynnwood Road, Pretoria, South Africa

Tel: +27 83 326 6549

Fax: +27 12 420 5048

walter.focke@up.ac.za

www.up.ac.za/chemeng

Abstract: Hydrated filler-type flame retardants were coated with approximately a monolayer of stearic acid using a solvent technique. Compared to the uncoated powders, the BET surface area was lower, the powder packing density was improved, and the thickening effect on white oil was significantly reduced. The latter two observations are rationalized in terms of a reduction in the attractive interactions between the powder particles. The viscosity of white oil slurries containing 25 wt % solids showed shear-thinning non-Newtonian behavior. The coated powders showed significantly lower viscosities at low shear rates although the difference diminished at high shear rates. The lower viscosities shown by the coated powders indicate that the surface modification facilitated the break-up of agglomerates and the dispersion of individual particles in the fluid.

***Keywords**: Rheology; viscosity; solid dispersion; flame retardant; surface characterization*

*To whom all correspondence should be addressed

1. Introduction

Polymers find increasing use as structural and functional materials. Owing to their combustible, organic nature, they pose a fire risk in some applications. This risk can be reduced by incorporating flame retardant additives. Laoutid et al. [1] provide a recent review of flame retardants for polymers. Hydrated fillers, e.g. aluminum trihydrate and magnesium hydroxide, have utility as endothermic flame retardants [2-4].

The candle model for polymer burning assumes independent pyrolysis and flame zones [5]. Heat transfer from the flame provides coupling between the gas and condensed phases. It drives the thermal degradation reactions that produce volatile fuel fragments that, in turn, feed the flame. This model suggests three possible strategies for flame proofing combustible polymers [5, 6]: (i) interference with the gas phase combustion and (ii) with the substrate pyrolysis reactions or (iii) their decoupling via a physical barrier to heat and mass transport. With endothermic flame retardants this may correspond to (i) dilution of the flammable gas with inert gases; (ii) the cooling of the substrate and promotion of charring; and (iii) the formation of an ash-char barrier layer. The endothermic decomposition reaction absorbs heat and releases inert gases [1, 4, 7]. The cooling of the polymer substrate inhibits the solid phase decomposition reactions. Simultaneously the steam and/or carbon dioxide released by the reaction dilutes the surrounding atmosphere with an inert gas.

The use of endothermic flame retardants is associated with some problems. In particular, on decomposition, $Mg(OH)_2$ forms a powdery residue with a high surface area [8]. It tends to catalyze oxidation of char residues leading to an afterglow effect. As a result, effective barrier formation is realized only when additional additives are incorporated [4, 9-11]. Secondly, high loadings are required to achieve adequate flame resistance [4]. The high filler loadings impair the fluidity of the corresponding melts [4, 14-16] and the mechanical properties of the solid compounds [4, 14]. Since these fillers are pulverized bulk materials, they tend to agglomerate during conveying and storage as a result of adhesive forces. When these agglomerates are added to a polymer, it is necessary that the compounding process succeeds in breaking down the agglomerates and thoroughly disperses the individual particles in the polymer melt [16]. A well-mixed homogeneous dispersion is required to minimize melt viscosity. The mechanical integrity of the compound is also compromised by the hydrophilic nature of these filler surfaces. Suitable surface modifications can improve the compatibility of inorganic fillers with hydrophobic polymer matrices [14]. Stearic acid is widely used to coat basic fillers such as calcium carbonate [17-20], magnesium hydroxide [14, 18, 21-23] and hydromagnesite [24]. Compounds containing stearate coated fillers show better processing behavior, increased elongation to break and improved impact properties at the cost of reduced tensile strength [12-14, 18, 25-26].

The degradation onset temperature for aluminum trihydrate is about 210 °C and it absorbs ca. 1.05 MJ/kg of heat [1]. Magnesium hydroxide is significantly more stable. Thermal decomposition occurs in the temperature range

280 °C to 350 °C and the enthalpy of decomposition is 1.2 - 1.3 MJ/kg [1, 27]. This allows magnesium hydroxide to be used in polymers requiring higher processing temperatures, e.g. nylon and polypropylene [28].

Magnesium carbonate and magnesium hydroxide ($Mg(OH)_2$) occur in nature as the minerals magnesite and brucite. Magnesium hydroxide has a layered structure composed of stacked trioctahedral metal hydroxide sheets. Hydrotalcite is a natural anionic clay mineral with the structural formula: $Mg_6Al_2(OH)_{16}CO_3.4H_2O$. However, in this study we consider a synthetic hydrotalcite-like compound with nominal composition $Mg_4Al_2(OH)_{12}CO_3.3H_2O$. Such synthetic analogues are commonly referred to as layered double hydroxides (LDH) [29-30]. They also feature the brucite-like stacked sheet structure of magnesium hydroxide [30]. The difference is that a portion of the magnesium ions in the sheets have been replaced with aluminum ions. This substitution imparts a net positive charge that is balanced by an equal negative charge from the interlayer carbonate anions [31]. Water molecules also occupy the interlayer space.

Hydrous carbonates and basic magnesium hydroxycarbonates are intermediate phases located between magnesium hydroxide and magnesium carbonate. Forms that occur as minerals [32] include nesquehonite ($MgCO_3{\cdot}3H_2O$) and lansfordite ($MgCO_3{\cdot}5H_2O$) [33], artinite ($MgCO_3{\cdot}Mg(OH)_2{\cdot}3H_2O$), hydromagnesite ($4MgCO_3{\cdot}Mg(OH)_2{\cdot}4H_2O$) and dypingite ($4MgCO_3{\cdot}Mg(OH)_2{\cdot}5H_2O$) [34]. At a unit cell level, these minerals also have a layer structure [33]. Magnesium hydroxide and magnesium carbonate are readily synthesized but it is very difficult to prepare pure, single phase basic magnesium carbonate forms. Nevertheless, Hayek and Gleispach [35] showed that pure hydromagnesite can be prepared by homogeneous precipitation and complex-acidolysis.

Camino et al. [27] compared the flame retardant effect of various inorganic hydroxides with that of hydrotalcite in poly(ethylene-co-vinyl acetate) (EVA). They found that EVA filled with 50 wt % flame retardant; the hydrotalcite-based compound featured the slowest heat release rate and the lowest evolved gas temperature. The basic carbonates, e.g. hydromagnesite, may offer fire retardancy performance comparable to magnesium hydroxide [1, 3, 25, 36-37]. While the enthalpy of decomposition is lower at ca. 0.80 MJ/kg [24], a greater quantity of inert gases including carbon dioxide is released.

This study is a first step in a project designed to explore the utility of magnesite ore-derived compounds as potential flame retardants for polymers. Powders were prepared on a pilot plant using proprietary processes and yielded small crystals in a profusely agglomerated state. Powders composed of such small agglomerated crystals are not suitable for compounding into polymer melts. They adversely affect the melt viscosity and the required loading levels can often not be achieved. However, owing to their high surface area, they are ideal for studying the effect of stearic acids coatings on physical properties. This investigation considers the effect of stearic acid coatings on the properties of such hydromagnesite and hydrotalcite powders as well as a magnesium hydroxide reference material. Finally, we follow Zhang et al. [15] and use mineral oil as model liquid to study the effect of the surface coating on the rheology of the particle suspensions.

2. Experimental

Materials

Hydromagnesite (grade HMH) and hydrotalcite (grade HT5) were supplied by Chamotte Holdings. The hydromagnesite was manufactured using a proprietary procedure based on the methods described by Botha and Strydom [38]. The hydrotalcite is a layered double hydroxide with the approximate composition $[Mg_{0.66}Al_{0.34}(OH)_2](CO_3)_{0.17}.½H_2O$. Both materials contained silica and magnesium carbonate as minor impurities. Magnesium hydroxide was obtained from Aldrich (Cat. No. 31,009-3 magnesium hydroxide 95%). Distilled water was used in all experiments. White oil, with a density of 0.831 g/cm^3 at 20 °C and a viscosity of 13.8 mPa.s at 40 °C, was obtained from Akulu Marchon. Acetone (99.5%) and stearic acid were supplied by Saarchem UnivAR and Bio-Zone Chemicals respectively. Potassium bromide (Uvasol KBr, Merck) was used to prepare samples for the recording of infrared spectra.

Stearic acid coating

Stearic acid surface coatings were applied using a solution method. A predetermined amount of stearic acid was weighed out into a 500 mL Schott Duran bottle. To this was added 400 mL of acetone. The sealed bottle was suspended in a water bath and shaken at regular intervals until all the stearic acid was fully dissolved. Then 20 g of inorganic filler (hydromagnesite, hydrotalcite or magnesium hydroxide) was added. The mixture was shaken manually for about one minute. Thereafter the contents were stirred for 30 minutes using a magnetic stirrer. The mixture was then allowed to stand for 3 days before recovering the filler and the solvent by filtering. The filtrates were dried at ambient temperature. In this way, the powders were exposed to solutions containing 0, 0.25, 0.50, 1.00, 2.50 and 5.00 g/L stearic acid in acetone. This corresponds to total stearic acid dosage levels corresponding to 0, 0.5, 1, 2, 5 and 10 wt % based on the mass of neat filler added. The actual amount of stearate absorbed on or by the fillers treated with the 2.5 g/L and 5 g/L solutions was determined by evaporating the recovered acetone solutions and weighing the residues.

Characterization

Particle size and BET surface area. Particle size distributions were determined using a Malvern Mastersizer Hydro 2000MU instrument. Single point BET surface area measurements were done using a Micromeritics Flowsorb II 2300 instrument.

Oil absorption. The oil absorption of neat powders, as well as powders treated with the 2.5 g/L stearic acid solution, was determined using the spatula rub-out method described in ASTM D 281-95.

Tap density. Tap density was determined by adding small amounts of powder to a 50 mL measuring cylinder. After each addition, the cylinder was exhaustively tapped against a wooden board at an angle of ca. 25 ° from the vertical to consolidate the column of powder. The mass of powder corresponding to a tapped volume of 50 mL was determined. The average of triplicate determinations is reported.

Scanning electron microscopy (SEM). Small quantities of powder were placed onto carbon tape on a metal sample holder. Excess powder was removed using a single compressed air blast. The samples were then coated with gold under argon gas using a SEM autocoating unit E5200 (Polaron equipment LTD). They were viewed on a JEOL 840 SEM scanning electron microscope under low magnification.

Thermal analysis. About 15 mg powder was placed in open 70 μL alumina pans. Thermogravimetric analysis was performed using the dynamic method on a Mettler Toledo A851 TGA/SDTA instrument in air flowing at a rate of 50 mL/min. Temperature was scanned from 25 to 900 °C at a rate of 10 °C/min.

X-Ray diffraction (XRD). XRD analysis on a PANalytical X-pert Pro powder diffractometer was used for phase identification. The instrument featured variable divergence and receiving slits and an X'celerator detector using Fe filtered Co Kα radiation (0.17901 nm). X'Pert High Score Plus software was used for data manipulation.

Diffuse Reflectance Infra-red Fourier Transform (DRIFT) analysis. Infrared spectra were recorded using a DRIFT accessory on a Perkin-Elmer Spectrum 2000GX FTIR spectrometer. The ratio of sample mass to KBr mass was set at 1:20. Thirty scans were recorded over the frequency range 400 - 4000 cm^{-1} and Fourier transformed at a resolution of 4 cm^{-1}.

Rheology. The white oil suspensions containing 25 wt % inorganic filler were prepared as follows: 2.250 g neat powder or 2.368 g of the 5 % stearic acid coated sample were mixed with 6.750 g and 6.632 g white oil respectively. The powders were thoroughly mixed into the liquid using an agate mortar and pestle. The viscosities of these white oil suspensions were measured at a temperature of 30 ºC on an Anton Paar Physica UDS 200 rheometer using the parallel plate geometry. The disk diameter was 25 mm and the gap between the two plates was set at 1.1 mm.

X-ray Photoelectron Spectroscopy (XPS). XPS spectra were obtained on a PHI spectrometer (Model 5400) equipped with an Mg/Al dual mode source and a small area analyzer with PSD detector. An achromatic Mg Kα X-Ray (1253.6 eV) source was operated at 300 W. The vacuum pressure was 10^{-8} torr during spectra acquisition. Survey spectra were obtained at take-off angles of 15ºC, 45ºC and 80ºC. Before analysis, samples were dried over P_2O_5 in a vacuum desiccator.

3. RESULTS

Figure 1 shows the morphology of the neat filler particles as observed by SEM. It shows that the hydrotalcite and the magnesium hydroxide powders comprise copiously agglomerated flake-like particles. The hydromagnesite consists of well-formed, dice-shaped crystals that appear glued-together by a less well-defined phase.

The Malvern particle size analysis of the all the powders revealed bimodal particle size distributions (PSD). The peak corresponding to the larger particle size is attributed to the presence of large agglomerates. The locations of the peaks at smaller particles sizes in the PSD probably give a better indication of primary particle dimensions. These were 1.5 μm, 1.0 μm and 5.8 μm for magnesium hydroxide, hydrotalcite and hydromagnesite respectively.

<Figure 1>
<Figure 2>

The XRD spectra in Figure 2 and the DRIFT spectra in Figure 3 confirm the chemical nature of the three powders. The sharp peaks in the XRD spectrum for $Mg(OH)_2$ and hydrotalcite point to high crystallinity of the corresponding powders. The peaks at $2\theta = 21.6$ ° and $2\theta = 13.5$ ° in the XRD spectra for magnesium hydroxide and hydrotalcite are consistent with the expected brucite layer basal spacings of 0.477 nm and 0.763 nm respectively. The XRD spectrum for the hydromagnesite shows additional reflections that indicate the presence of dypingite and magnesite as impurity phases.

The $Mg(OH)_2$ DRIFT spectrum shown in Figure 3 is characterized by a sharp and intense –OH stretching vibration peak at ca. 3700 cm^{-1}. This sharp peak is also observed in the hydromagnesite at about 3650 cm^{-1} but in the hydrotalcite it is much broader and it is centered at a lower wavenumber (ca. 3450 cm^{-1}). The hydrotalcite features a single carbonate peak at 1367 cm^{-1} while in the hydromagnesite the carbonate asymmetric stretching vibration band is split with peaks at 1420 and 1480 cm^{-1}. The latter also features a carbonate symmetric stretch band at ca. 1120 cm^{-1} and three bending bands at 800 cm^{-1}. The presence of the water of crystallization is indicated by the bands at ca. 3510 and 3450 cm^{-1} [32].

<Figure 3>
<Figure 4>

Figure 4 compares the infrared spectra of hydromagnesite, with and without a stearic acid coating, with those for stearic acid and magnesium stearate. The small peaks at ca. 2915 and 2855 cm^{-1} (due to symmetric and asymmetric stretching vibration of aliphatic groups $-CH_2-$ groups) confirms the presence of stearic acid in the coated sample. The spectrum for stearic acid shows the carbonyl stretching vibration at ca. 1700 cm^{-1}. Unfortunately the low

intensity of the absorption bands in the present hydromagnesite spectrum makes it impossible to establish the nature of the absorbed stearic acid, i.e. whether neutral or ionized.

Comparison of the DRIFT spectra for the stearic acid coated and uncoated magnesium hydroxide and hydrotalcite samples showed similar small peaks at ca. 2915 and 2855 cm^{-1} for the stearic acid solution treated samples. The absence of such peaks for the uncoated samples, confirms the presence of stearic acid on the surface of the coated samples.

Figure 5 shows mass loss curves for hydromagnesite, magnesium hydroxide and hydrotalcite powders obtained in air. The degradation pathways for these three compounds are given in Schemes I to III. In each case water, or water and carbon dioxide are released in gaseous form and inert oxides remain.

<Figure 5>

$$Mg(OH)_2 \rightarrow MgO + H_2O\uparrow$$

Scheme I. Thermal decomposition of magnesium hydroxide. The theoretical mass loss is 30.9 wt %.

$$[Mg_4Al_2(OH)_{12}]CO_3{\cdot}3H_2O$$
$$\downarrow \quad \text{dehydration 120 - 250°C}$$
$$Mg_4Al_2(OH)_{12}]CO_3 + 3H_2O\uparrow$$
$$\downarrow \quad \text{dehydroxylation \& decarbonation 250 - 550°C}$$
$$4\,MgO + Al_2O_3 + 6H_2O\uparrow + CO_2\uparrow$$

Scheme II: Thermal decomposition of the synthetic hydrotalcite [39-40].

$$4MgCO_3.Mg(OH)_2.4H_2O$$
$$\downarrow \quad \text{dehydration < 150°C}$$
$$4MgCO_3.Mg(OH)_2.2H_2O + 2H_2O$$
$$\downarrow \quad \text{dehydration < 250°C}$$
$$4MgCO_3.Mg(OH)_2 + 2H_2O\uparrow$$
$$\downarrow \quad \text{dehydroxylation 250 - 350°C}$$
$$4MgCO_3.MgO + H_2O\uparrow$$
$$\downarrow \quad \text{decarbonation 350 - 550°C}$$
$$4MgCO_3.MgO \rightarrow 5MgO + 4CO_2\uparrow$$

Scheme III: Degradation pathway for hydromagnesite [41-44].

The mass loss of the hydrotalcite sample proceeds stepwise with three distinct but overlapping peaks in the DTG trace. These events are commonly attributed to the loss of interlayer water, dehydroxylation and a combination dehydroxylation-decarbonation reaction respectively [40].

The endothermic decomposition of hydromagnesite occurs in three steps over the temperature range 200°C to 550°C as shown in Scheme III [43]. The first step entails the removal of water of crystallization. Water is also released in the second step owing to the decomposition of magnesium hydroxide layers. Finally carbon dioxide is released when the $MgCO_3$ decomposes to form MgO.

The residual masses at the end temperatures indicated in Figure 5 were 69.3 wt %, 58.1 wt % and 45.3 wt % for $Mg(OH)_2$, hydrotalcite and hydromagnesite respectively. The corresponding theoretically expected values are 69.1 wt %, 56.1 wt % and 43.1 wt % for $Mg(OH)_2$, hydrotalcite and hydromagnesite respectively. The small discrepancies are attributed to the presence of impurities.

TG was also used to estimate the amount of stearate absorbed on the powders that were treated with 2.5 g/L and 5 g/L stearic acid solutions. The method assumes that the stearate is completely lost at elevated temperatures. The calculation procedure compared the relative mass loss of the coated sample to that of the neat powder at high temperature (e.g. 800 ºC), but adjusted with respect to the mass loss observed at 150 ºC to correct for the possibility of variable moisture contents. The results are presented in Table 1.

Figure 6 shows the effect of stearic acid coating on the measured BET surface areas. A decrease in BET surface area is observed as the stearic acid concentration in the solution is increased. However, above 1 g/L the BET surface areas reached plateau values of 6.9 m^2/g, 10 m^2/g and 23 m^2/g for magnesium hydroxide, hydrotalcite and hydromagnesite respectively. This reduction is probably caused by the stearic acid filling in some narrow crevice defects in the plate-like crystals.

<Figure 6>

Close-packed stearic acid chains assume a hexagonal arrangement with the extended chains oriented at an angle 29° to the vertical [45]. The projected surface area per stearate chain is approximately equal to 0.22 nm^2 [46]. If the available surface area of the powder is completely covered by such a monolayer, the amount absorbed is given by 0.215 A_{BET} wt %. The measured BET surface areas (A_{BET}) for the neat powders were 8.2 m^2/g, 17.3 m^2/g and 34.5 m^2/g for $Mg(OH)_2$, hydrotalcite and hydromagnesite respectively. This implies monolayer coverage would be attained at 1.8 wt %, 3.7 wt % and 7.3 wt % respectively. These values are compared to measured values in Table 1. The results indicate that the actual amount absorbed from solutions containing 2.5 g/L or more stearic acid was slightly below the value expected for monolayer coverage in the case of hydrotalcite and hydromagnesite. The results also suggest that the coverage on the magnesium hydroxide exceeded monolayer absorption.

<Table 1>

Figure 7 shows the carbon to oxygen (C/O) atomic ratio calculated from the peak areas of the C1s (285-295 eV) and O1s (530-545 eV) signals as measured by XPS. The XPS technique samples the composition of the matter at the surface to a depth of a few nanometers. Stearic acid has a theoretical C/O atomic ratio of approximately 9.0. The value obtained by XPS analysis for the grade stearic acid used presently was actually 9.5. These values are much higher that the theoretical ratios for the neat hydrotalcite (0.056) and neat hydromagnesite (0.222). The ratios measured for coated samples thus provide an indication of the amount of stearic acid absorbed on the surfaces of the powders. The C/O atomic ratio initially increases rapidly with the stearic acid solution concentration but then levels off above 2.5 g/L. Values similar to that expected for neat stearic acid were attained for the hydromagnesite and hydrotalcite samples treated with a solution containing 2.5 g/L stearic acid. This suggests that close to monolayer coverage was achieved and it was therefore decided to use these samples in the rheology experiments. The XPS data indicates a value for the C/O atomic ratio that is approximately equivalent to two thirds of that for stearic acid for the $Mg(OH)_2$ treated with the 2.5 g/L solutions and equivalent to nine tenths of that for stearic acid for the $Mg(OH)_2$ treated with the 5.0 g/L solution. This is at odds with the TG and solution depletion estimates shown in Table 1. Both these techniques suggest that the stearic acid adsorbed about 50 % more than a monolayer equivalent (with the $Mg(OH)_2$ treated with the 2.5 g/L solution having a higher organic content). The reason for these discrepancies is not understood at present. It is possible that the "missing" stearic acid was incorporated as a bulk phase in crevices internal to the $Mg(OH)_2$ particles.

Figure 8 shows specific filler volume fractions measured using the tap density techniques and the oil absorption technique. The values determined using the tap density method are significantly lower than those calculated from oil absorption measurements. This is understandable as in this method the particles are compacted in a virtually shear-free manner. The oil absorption procedure involves application of significant shear with the oil acting as a lubricant. This helps to break-up loose particle agglomerates allowing the particles to pack more efficiently. The presence of a stearic acid coating is clearly beneficial yielding significantly higher packing densities compared to the neat fillers. The improvement was greatest in the case of the hydrotalcite and least for the magnesium hydroxide.

<Figure 7>
<Figure 8>

Figure 9 shows the viscosity of the white oil and suspensions containing 25 wt % inorganic filler as measured at a temperature of 30 ºC. Note that the indicated filler content refers to the purely inorganic part, i.e. the stearic acid coating was deemed to form part of the organic liquid phase. Owing to the large difference in densities between the solids and the liquid medium, the volume fraction filler in the suspensions amounted to only 10.3, 11.0 and 11.9 volume % for $Mg(OH)_2$, hydromagnesite and hydrotalcite respectively.

<Figure 9>

The white oil shows the expected Newtonian behavior with a shear-independent viscosity of 21.7 mPa.s. The viscosities of the slurries are much higher, by several orders of magnitude, when compared at a shear rate of 1 s^{-1}. However, the slurry viscosities also show strong shear-thinning behavior. The relative viscosity for the $Mg(OH)_2$ slurry decreases to about 3.0 at a shear rate of 1000 s^{-1}. Shear thinning non-Newtonian behavior is well known for concentrated suspensions but in this instance such behavior is observed at the relatively low solid phase volume fraction of 0.10 to 0.12. This implies that the fine powders considered here are very effective thickening agents for white oil. This is especially true for the uncoated hydromagnesite and hydrotalcite powders.

Furthermore, close to identical data were generated for a decrease in shear rate. A plot of the values for a decreasing shear rate (reverse) fit the increasing shear rate (forward) plots in Figure 9 almost identically; showing no form of hysteresis. This implies that the mechanism for the reduction in viscosity due to an increase in shear rate is reversible and not permanent.

The shear thinning behavior of the hydromagnesite and hydrotalcite suspensions follow the power-law model with:

$$\eta = K\dot{\gamma}^{n-1} \qquad (1)$$

Values for the consistency index *K* and the flow behavior index *n* were calculated and are presented in Table 2. Both parameters change when a stearic acid coating is applied. The consistency index decreases by about an order of magnitude for the hydrotalcite and the hydromagnesite. These changes reflect the decrease in slurry viscosity for the coated powders compared to the neat uncoated versions.

<Table 2>

4. DISCUSSION

The viscosity of particle suspensions depends on the nature of the flow units present [47]. The flow units may comprise individually dispersed powder particles or particle agglomerates that act in unison with occluded liquid. Any such associated liquid contributes to the effective volumetric concentration of the flow units in the remaining liquid. In other words, the occluded liquid behaves in such a way that it becomes part of the “solid” phase. The Newtonian viscosity of such suspensions is adequately described by the Krieger-Dougherty [47-49] expression:

$$\eta_r = \frac{\eta}{\eta_o} = \left(1 - \frac{\varphi}{\varphi_{max}}\right)^{-2.5k\varphi_{max}} \quad (2)$$

Here η_o represents the viscosity of the pure fluid, η that of the suspension, and η_r is the relative viscosity. k is a particle shape factor that assumes the value unity for spheres [47]. φ is the volume fraction of the flow units and φ_{max} is the maximum attainable volume fraction. At this level an abrupt transition to elastic solid-like behavior is observed [50].

Eilers' [51-52] expression provides an alternative formulation that gives very similar results to the Krieger-Dougherty model [48-49]:

$$\eta_r = \left(1 + \frac{1.25k\varphi}{1 - \varphi/\varphi_{max}}\right)^2 \quad (3)$$

Real slurries show non-Newtonian flow characteristics with the apparent viscosity decreasing with increasing rate of shear [48]. This is commonly attributed to their agglomerative nature [53]. When the individual particles are suspended in a liquid, they aggregate to form floc-like agglomerates or clusters. Newtonian behavior is observed when the agglomerates, acting as individual flow units, retain their integrity. Non-Newtonian behavior results when the application of shear induces changes in the effective volume of these flow units [47-49, 53]. Quemada [54] and Wildemuth and Williams [55] independently posed that the incorporation of a shear-dependent maximum packing fraction (φ_{max}) in the rheological model for viscosity suffices to explain virtually all non-Newtonian effects over the entire concentration range. At low shear the agglomerates assume a loose floc structure that imbibes much of the fluid. The shear-thinning behavior observed at intermediate deformation rates is then a manifestation of the shear induced reduction of the degree of aggregation and concomitant release of occluded fluid [56]. There are two distinct mechanisms for such agglomerate break-up: erosion and rupture [57, 58]. In erosion individual particles are removed from the cluster and dispersed into the fluid. In the rupture mechanism, the agglomerate breaks down into fragments of similar size. The critical stress for effecting erosion tends to be smaller than that required for rupture. When complete cluster break-up is achieved, the slurry viscosity coincides with the predictions of equations (2) or (3) with φ_{max} defined by the maximum packing density of the individual particles [53] and this corresponds to a packed bed scenario. Experimental [50] and theoretical [59] studies indicate that the maximum three-dimensional random close packing density of monodisperse spheres corresponds to $\varphi_{max} = 0.64$.

Usui [60] argues that the clusters assume a spherical shape when the number of primary particles in the clusters becomes large. In addition, it is assumed here that the clusters are of similar size. It is then possible to estimate a lower limit for the porosity of the agglomerates present at low shear rates using either equation (2) or equation (3).

The hydrodynamic volume of the agglomerates depends on their porosity (ε), i.e. how loosely the particles are packed inside the flocs. For hydrotalcite and hydromagnesite the observed relative viscosities exceeded 500 at the lowest shear rates investigated. These values are so much higher than unity that for all practical purposes both equations indicate that the porosity can be estimated using:

$$\varepsilon = 1 - \varphi/\varphi_{max} = 1 - \varphi/0.64 \qquad (4)$$

This yields values of 0.81 and 0.83 for the uncoated hydrotalcite and hydromagnesite samples respectively. These values are similar to the porosity value obtained for both samples using the tap density technique, i.e. 0.81. The implication is that the flocs, present at low shear, have a packing density similar to remnants of the original dry agglomerates. This is rather surprising given that the suspensions were prepared by a high shear process. Therefore the evidence suggests that, despite being well dispersed during the preparation step, they have a natural tendency to revert to an agglomerated floc structure with porosities similar to those of the solid dry powders. Further proof of this re-agglomeration tendency is the reversibility of the viscosity plots for an increase and decrease in the shear rate. Reducing the shear rate allows the particles to re-agglomerate to an agglomerated floc structure and manifests as an increase in viscosity.

The neat stearic acid coated magnesium hydroxide slurries attain a Newtonian viscosity plateau at shear rates exceeding 100 s^{-1}. It can be assumed that this state corresponds to the state where all the particles are individually dispersed so that the maximum packing is given by the oil absorption value, i.e. $\varphi_{max} = 0.447$. This allows one to estimate the shape factor k to be estimated using either equation (2) or (3). The Krieger-Dougherty equation and Eilers' model yield similar values of $k = 3.39$ and $k = 3.86$ respectively.

The fact that the stearic acid coated powders yield slurries with significantly lower viscosities indicates that the surface treatment makes it easier for agglomerates to break-up under the influence of shear. This in turn suggests that the adhesive forces between particles have been weakened by the stearic acid coating.

5. CONCLUSION

The effect of a stearic acid coating on the properties of hydrated filler-type flame retardants was studied. The flame retardants comprised fine synthetic powders of magnesium hydroxide hydromagnesite and hydrotalcite. The surface coating was applied by treating the powders with dilute solutions of stearic acid in acetone. The presence of the coating was confirmed by DRIFT and quantified by XPS and TG. It was found that the coating level approximately equivalent to monolayer coverage was achieved when the hydrotalcite and hydromagnesite powders were treated with 20 mL acetone/g filler containing 2.5 g/L stearic acid.

Measured BET surface areas of the hydrotalcite and hydromagnesite powders decreased by as much as 33% when coated with stearic acid. SEM showed that the hydrotalcite and magnesium hydroxide powders comprised small crystals that are profusely agglomerated. Owing to their fineness and tendency to agglomerate in high porosity structures, both the hydrotalcite and hydromagnesite powders are very effective thickening agents for white oil. The rheology of slurries containing 25 wt % solids (ca. 11 volume %) was studied as a function of shear rate. The suspended powders increased the apparent low-viscosity by several orders of magnitude. This substantial thickening effect is attributed to a tendency of the particles to aggregate as high-porosity flocs in the oil. A lower limit for the porosity of the flocs is estimated at 81 volume % on the assumption that the flocs are spherical in shape and similar in size.

The suspensions also showed considerable shear thinning. This is consistent with the idea that the application of shear causes break-up of the agglomerates and releases the occluded fluid. The significantly lower viscosities observed for the stearic acid treated samples indicate that the surface coating reduces the adhesive forces between the particles. This makes it easier to break-up the agglomerates and aids dispersion of individual particles. However, a reduction in the shear rate allows for the reformation of the agglomerates.

Acknowledgements

Financial support for this research, from the Institutional Research Development Programme (IRDP) of the National Research Foundation of South Africa (NRF) and the THRIP program of the Department of Trade and Industry (administered by the NRF), is gratefully acknowledged.

6. REFERENCES

1. Laoutid F, Bonnaud L, Alexandre, M (2009) New prospects in flame retardant polymer materials: From fundamentals to nanocomposites. Mater Sci Eng, R 63(3):100-125
2. Delfosse L, Baillet C, Brault A, Brault, D (1989) Combustion of ethylene-vinyl acetate copolymer filled with aluminium and magnesium hydroxides. Polym Degrad Stab 23(4):337-347
3. Horn WE (2000) Inorganic hydroxides and hydroxycarbonates: Their function and use as flame-retardant additives. 293-294 In: Grand AF (ed), Wilkie CA (ed) Fire Retardancy of Polymeric Materials, 1st Ed. CRC Press, Boca Raton
4. Hornsby PR (2001) Fire retardant fillers for polymers. Int Mater Rev 46(4):199-210
5. Fenimore CP, Jones GW (1966) Modes of inhibiting polymer flammability. Comb and Flame, 10(2):295-301
6. Fenimore CP, Martin FJ (1966) Flammability of polymers. Comb and Flame, 10(2):135-139

7. Hornsby PR, Watson CL (1989) Mechanism of smoke suppression and fire retardancy in polymers containing magnesium hydroxide filler. Plast Rubber Process Appl 11(1):45-51
8. Hornsby PR, Watson CL (1990) A study of the mechanism of flame retardance and smoke suppression in polymers filled with magnesium hydroxide. Polym Degrad Stab 30(1):73-87
9. Carpentier F, Bourbigot S, Le Bras M, Delobel R, Foulon M (2000) Charring of fire retarded ethylene vinyl acetate copolymer - magnesium hydroxide/zinc borate formulations. Polym Degrad Stab 69(1):83-92
10. Genovese A, Shanks (2007) RA Structural and thermal interpretation of the synergy and interactions between the fire retardants magnesium hydroxide and zinc borate. Polym Degrad Stab 92(1):2-13
11. Burns M, Wagenknecht U, Kretzschmar B, Focke WW (2008) Effect of hydrated fillers and red phosphorus on the limiting oxygen index (LOI) of EVA-PVB and LDPE-EVAL blends. J Vinyl Add Tech 14:113-119
12. Hornsby PR (1999) Rheology, compounding and processing of filled thermoplastics. Adv Polym Sci 139:155-217
13. Hornsby PR (1994) Application of magnesium hydroxide as a fire retardant and smoke-suppressing additive for polymers. Fire Mater 18(5):269-276
14. Wang Z, Chen Z, Fan W, Nie W (2006) Effects of surface modifiers on mechanical and rheological properties of halogen-free flame retarded polyethylene composites. Polymer Plast Tech Eng 45(2):191-196
15. Zhang F, Zhang H, Su Z (2007) Surface treatment of magnesium hydroxide to improve its dispersion in organic phase by the ultrasonic technique. Appl Surf Sci 253(18):7393-7397
16. Potente H, Flecke J, (1997) The breaking down and agglomerating of fillers in polymer melt: A physical model for mathematical description. J Reinf Plas Compos 16(14) 1281-1292
17. Papirer E, Schultz J, Turchi C (1984) Surface properties of a calcium carbonate filler treated with stearic acid. Eur Polym J 20:1155-1158
18. Gilbert M, Petiraksakul P (1997) Stearate coatings on particulate fillers - The effects on resulting compound properties. Polym and Polym Compos 5(8):535-539
19. Osman M, Suter U (2002) Surface Treatment of Calcite with Fatty Acids: Structure and Properties of the Organic Monolayer. Chem Mater 14:4408-4415
20. Khanna, YP, Taylor DA, Paynter CD, Skuse DR (2009) Surface modification of calcium carbonate. I. Characterization of physico-chemical phases of stearic acid coating. Submitted to J Mater Sci
21. Liauw CM, Rothon RN, Hurst SJ, Lees GC (1998) The use of flow micro-calorimetry and FTIR techniques for characterising filler/organic acid interactions. Compos Interfaces 5(6):503-514
22. Gilbert M, Sutherland I, Guest A (2000) Characterization of coated particulate fillers. J Mater Sci 35(2):391-397
23. Gilbert M, Petiraksakul P, Mathieson I (2001) Characterisation of stearate/stearic acid coated fillers. Mater Sci Technol 17(11):1472-1478
24. Haurie L, Fernández AI, Velasco JI, Chimenos JM, Ticó-Grau JR, Espiell F (2005) Synthetic hydromagnesite as flame retardant. A study of the stearic coating process. Macromol Symp 221:165-174

25. Rigolo M, Woodhams RT (1992) Basic magnesium carbonate flame retardants for polypropylene. Polym Eng Sci 32:327-334
26. Huang H, Tian M, Yang J, Li H, Liang W, Zhang L, Li X (2008) Stearic acid surface modifying Mg(OH)2: Mechanism and its effect on properties of ethylene vinyl acetate/Mg(OH)2 composites. J Appl Polym Sci 107(5):3325-3331
27. Camino G, Maffezzoli A, Braglia M, De Lazzaro M, Zammarano M. (2001) Effect of hydroxides and hydroxycarbonate structure on fire retardant effectiveness and mechanical properties in ethylene-vinyl acetate copolymer. Polym Degrad Stab 74(3):457-464
28. Miyata S, Imahashi T, Anabuki H (1980) Fire-retarding polypropylene with magnesium hydroxide. J Appl Polym Sci, 25(3):415-425
29. Miyata S, Kumura, T. (1973) Synthesis of new hydrotalcite-like compounds and their physico-chemical properties, Chem Lett 843-848
30. Bellotto M, Rebours B, Clause, O Lynch J (1996) A re-examination of hydrotalcite crystal chemistry. J Phys Chem 100:8524-8527
31. De Roy A, Forano C, El Malki K, Besse J P (1992) In: Occelli ML (ed), Robson HE (ed), Expanded Clays and Other Microporous Solids, 1st edn. Van Nostrand Reinhold, New York, 2:108
32. White W B (1971) Infrared characterization of water and hydroxyl ion in the basic magnesium carbonate minerals. Am Mineral 56:46-53
33. Hales MC, Frost RL, Martens, WN (2008) Thermo-Raman spectroscopy of synthetic nesquehonite – implication for the geosequestration of greenhouse gases. J Raman Spectrosc 39:1141-1149
34. Raade G (1970) Dypingite, a new hydrous basic carbonate of magnesium, from Norway. Am Mineral 55(9-10):1457-1465
35. Hayek E, Gleispach H (1966) Hydroxidcarbonate von Magnesium und Zink – (Präparative Homogenfällung durch Komplexacidolyse, 5. Mitt.) Monatsh Chem 97(4):1059-1063
36. Haurie L, Fernández AI, Velasco JI, Chimenos JM, Lopez Cuesta JM, Espiell F (2006) Synthetic hydromagnesite as flame retardant. Evaluation of the flame behaviour in a polyethylene matrix. Polym Degrad Stab 91(5): 989-994
37. Morgan AB, Cogen JM, Opperman RS, Harris JD (2007) The effectiveness of magnesium carbonate-based flame retardants for poly (ethylene-co-vinyl acetate) and poly (ethylene-co-ethyl acrylate). Fire and Mater 3(6):387-410
38. Botha A, Strydom CA (2001) Preparation of a magnesium hydroxy carbonate from magnesium hydroxide. Hydrometallurgy 62(3):175-183
39. Rey F, Fornés V, Rojo JM (1992) Thermal decomposition of hydrotalcites. An infrared and nuclear magnetic resonance spectroscopic study. J Chem Soc, Faraday Trans 88:2233-2238
40. Bera P, Rajamathi M,Hegde MS, Kamath PV (2000) Thermal behavior of hydroxides, hydroxysalts and hydrotalcites. Bull Mater Sci 23:141-145

41. Sawada Y, Yamaguchi J, Sakurai O, Uematsu K, Mizutani N, Kato M (1979) Thermogravimetric study on the decomposition of hydromagnesite $4MgCO{\cdot}Mg(OH){\cdot}4H_2O$. Thermochim Acta 33:127-140
42. Sawada Y, Yamaguchi J, Sakurai O, Uematsu K, Mizutan N, Kato M (1979) Thermal decomposition of basic magnesium carbonates under high-pressure gas atmospheres. Thermochim Acta 32(1-2):277-291
43. Choudhary VR, Pataskar SG, Gunjikar VG, Zope GB (1994) Influence of preparation conditions of basic magnesium carbonate on its thermal analysis. Thermochim Acta 232:95-110
44. Vágvölgyi V, Frost RL, Hales M, Locke A, Kristóf J, Horváth E (2008) Controlled rate thermal analysis of hydromagnesite. J Therm Anal Calorim 92(3):893-897
45. Itoh T, Ohta N, Shichi T, Yui T Takagi K (2003) The self-assembling properties of stearate ions in hydrotalcite clay composites, Langmuir 19:9120-9126
46. He JX, Yamashita S, Jones W, Yamagishi A (2002) Templating effects of stearate monolayer on formation of Mg-Al-hydrotalcite, Langmuir 18:1580-1586
47. Mandersloot WGB, Scott KJ (1990) Rheology of particle suspensions. S Afr J Chem Eng 2:53-69
48. Krieger IM, Dougherty TJ (1959) A Mechanism for Non-Newtonian Flow in Suspensions of Rigid Spheres. Trans of the Soc Rheol 3:137-152
49. Krieger (1972) Rheology of monodisperse lattices. Adv Colloid Interface Sci 3(2):111-136
50. Jones DAR, Leary B, Boger DV (1991) The rheology of a concentrated colloidal suspension of hard spheres. J Colloid Interface Sci, 147(2):479-495.
51. Eilers H (1941) Die Viskosität von Emulsionen hochviskoser Stoffe als Funktion der Konzentration. Kolloid-Z 97(3): 313-321
52. Eilers H (1943) Die Viskositäts-Konzentrationsabhängigkeit kolloider Systeme in organischen Lösungsmitteln. Kolloid-Z 102(2):154-169
53. Usui H, Kishimoto K Suzuki H (2001) Non-Newtonian viscosity of dense slurries prepared by spherical particles. Chem Eng Sci 56(9):2979-2989
54. Quemada D (1986) Comments on the paper "Viscosity of suspensions modeled with a shear-dependent maximum packing fraction" by Wildemuth CR, Williams MC Rheol Acta 25(6):647-649
55. Wildemuth CR, Williams MC (1984) Viscosity of suspensions modeled with a shear-dependent maximum packing fraction. Rheol Acta 23(6):627-635
56. Tsenoglou C (1990) Scaling concepts in suspension rheology. J. Rheol. 34(1):15-24
57. Rwei SP, Manas-Zloczower I, Feke DL (1990) Observation of carbon black agglomerate dispersion in simple shear flows. Polym Eng Sci 30(12):701-706
58. Hansen S, Khakhar DV, Ottino JM (1998) Dispersion of solids in nonhomogeneous viscous flows. Chem Eng Sci 53(10):1803-1817
59. Jalali P, Li M (2004) An estimate of random close packing density in monodisperse hard spheres. J Chem Phys 120(2):1138-1139
60. Usui H (2002) Prediction of dispersion characteristics and rheology in dense slurries. J Chem Eng Jpn 35(9):815-829

List of Tables

List of Figures

Table 1. Stearic acid coating levels expressed in wt % as calculated from the residual level in the solvent and from TG data.

Powder:	hydrotalcite		$Mg(OH)_2$		hydromagnesite	
Stearic acid solution concentration, g/L	solvent analysis	TG	solvent analysis	TG	solvent analysis	TG
2.5	2.5±0.3	2.8	3.3±0.2	2.9	5.1±0.0	-
5.0	3.6±0.4	3.2	2.8±0.1	2.1	5.6±0.0	6.4
Monolayer estimate (BET)	3.7		1.8		7.3	

Table 2. Consistency index *K* and the flow behaviour index *n* for the slurries

Powder:	hydrotalcite		$Mg(OH)_2$		hydromagnesite	
Treatment	*K*	*n*	*K*	*n*	*K*	*n*
Neat	105	0.03	1.64	0.24	165	0.28
Coated (2.5 g/L)	16.3	0.17	-	-	12.7	0.18

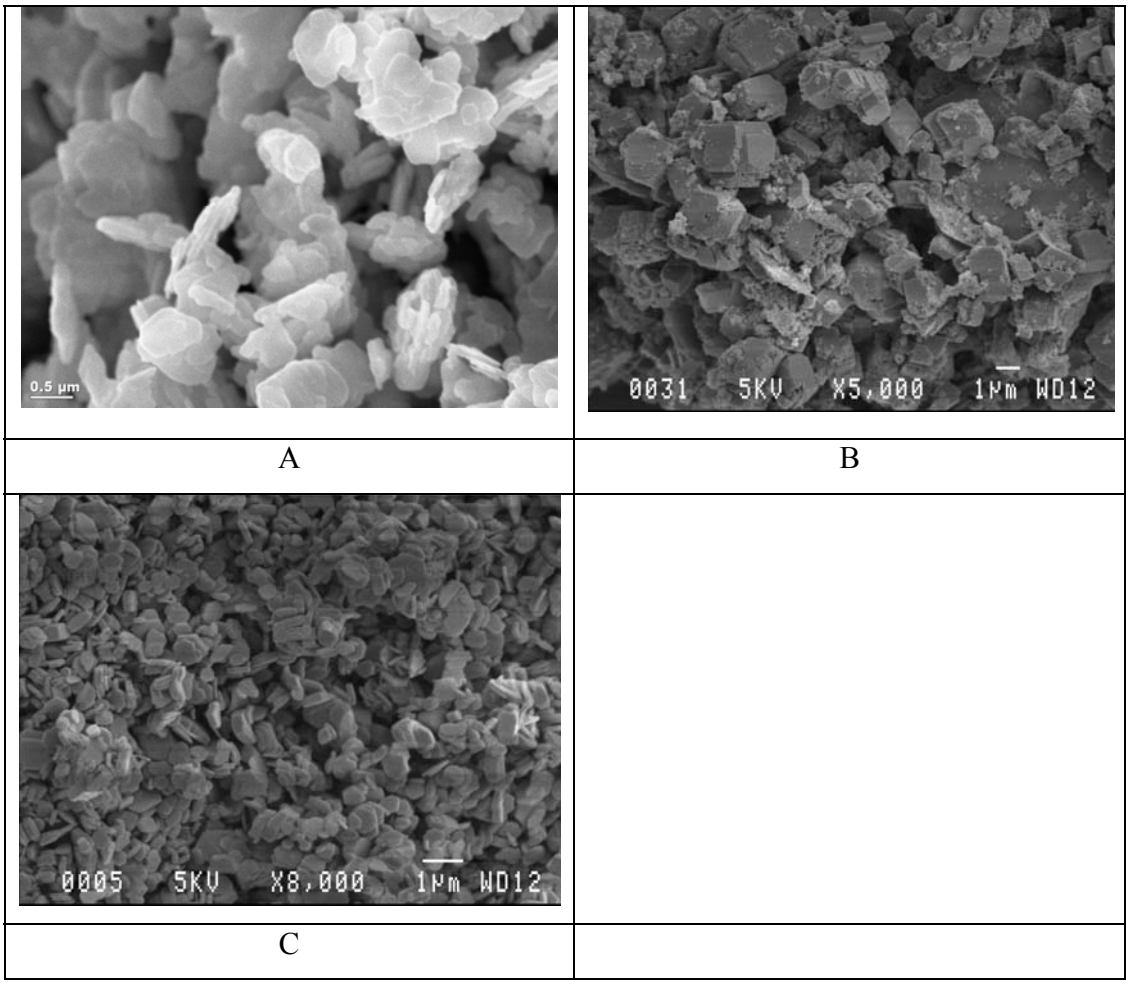

Figure 1. SEM pictures showing the morphology of the neat powders: A. Hydrotalcite. B. Hydromagnesite. C. Magnesium hydroxide.

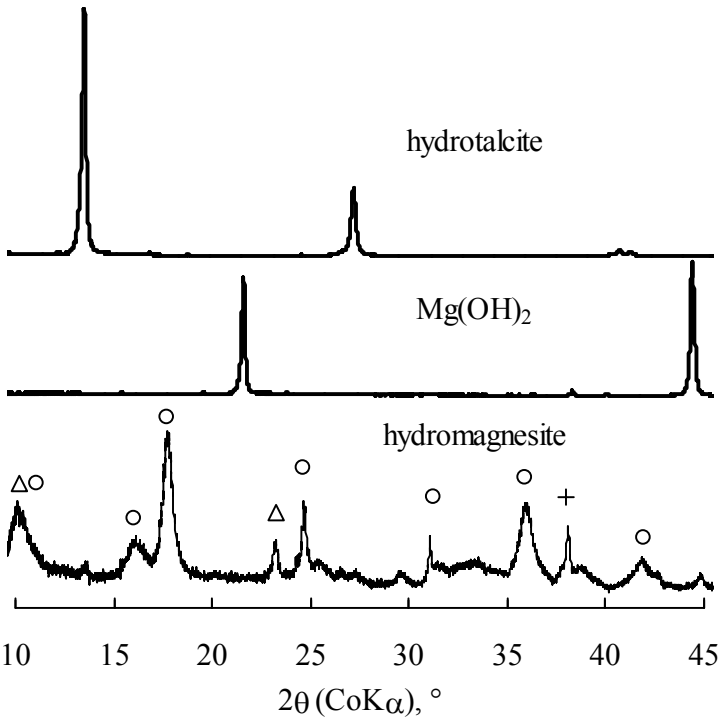

Figure 2. XRD spectra of the various powders. Key: hydromagnesite (◦), dypingite (Δ) and magnesite (+).

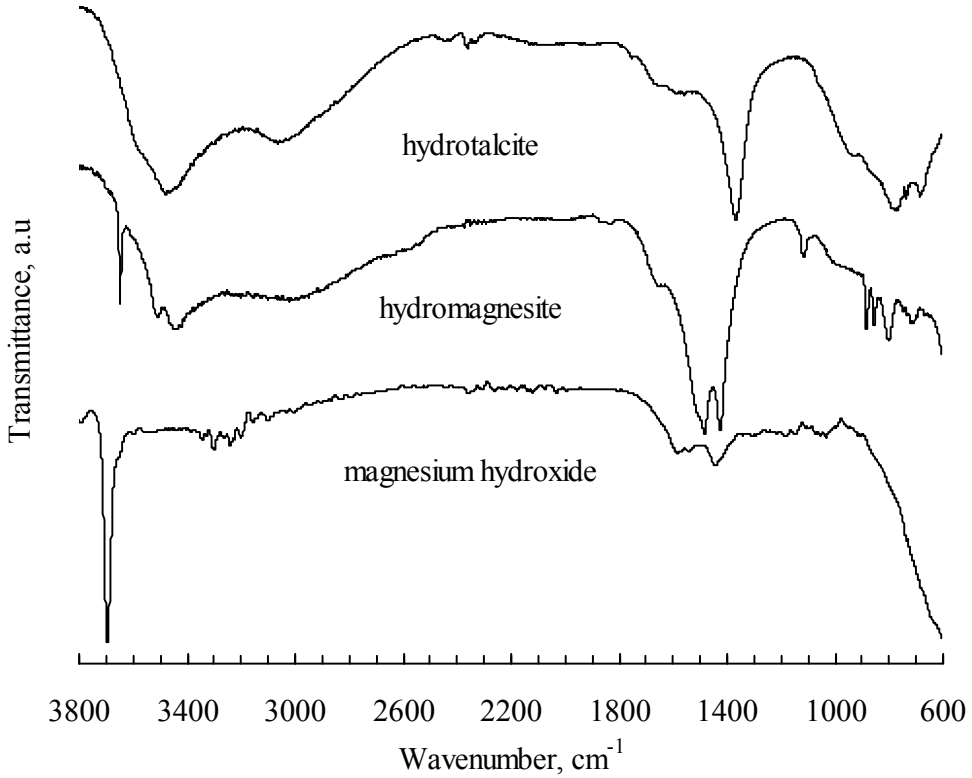

Figure 3. DRIFT spectra for magnesium hydroxide, hydrotalcite and hydromagnesite.

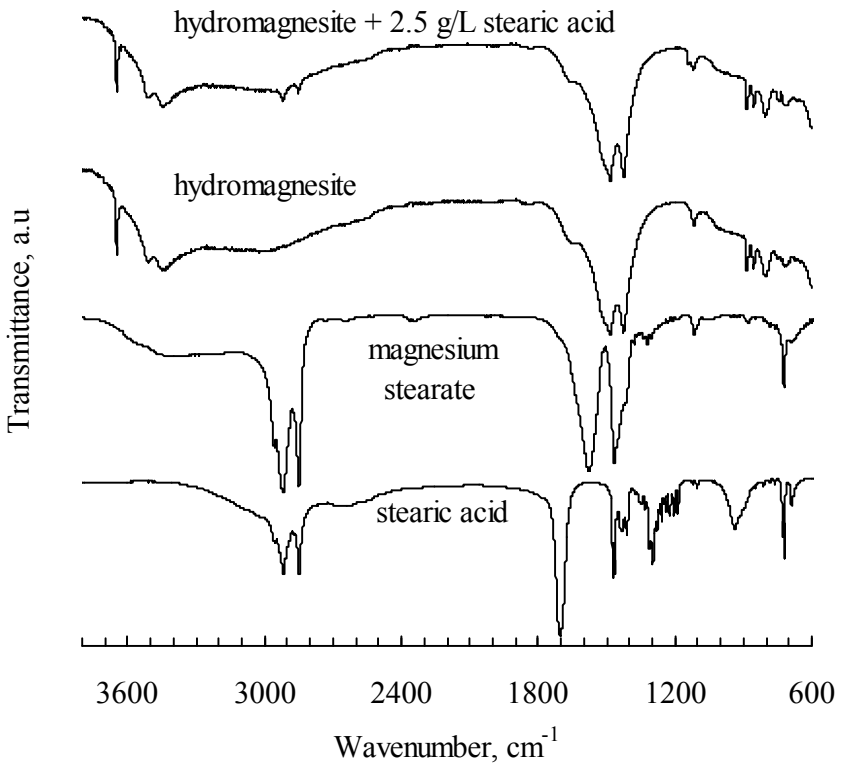

Figure 4. DRIFT spectra for neat and 2.5 g/L stearic acid solution treated hydromagnesite compared to those for magnesium stearate and neat stearic acid.

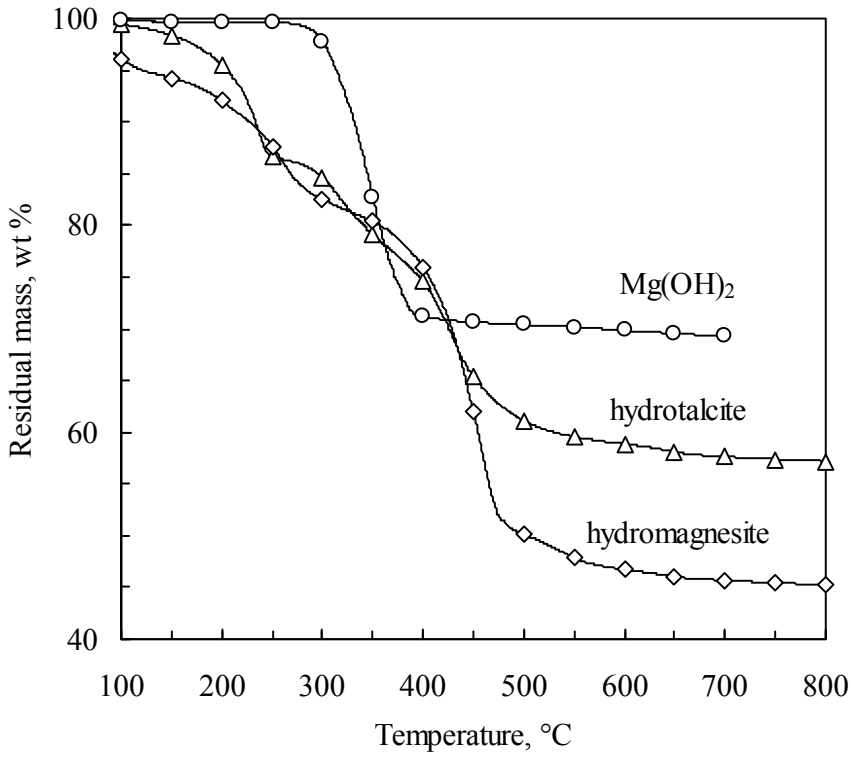

Figure 5. TG curves for hydromagnesite, magnesium hydroxide and hydrotalcite powders obtained in air at a scan rate of 10°C/min.

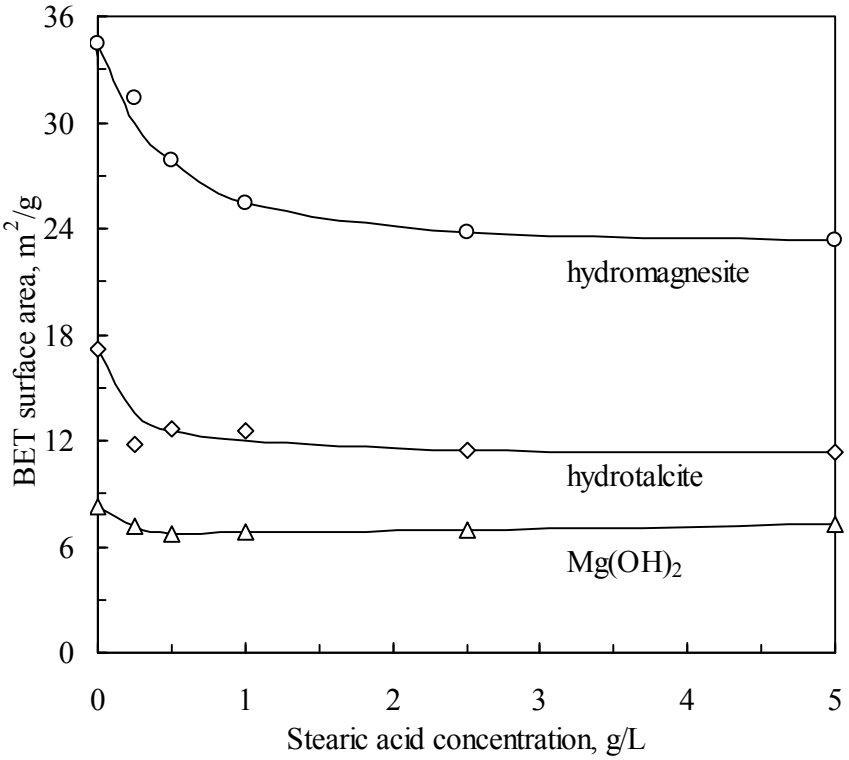

Figure 6. Effect of stearic acid dosage level on the BET surface area of the powders.

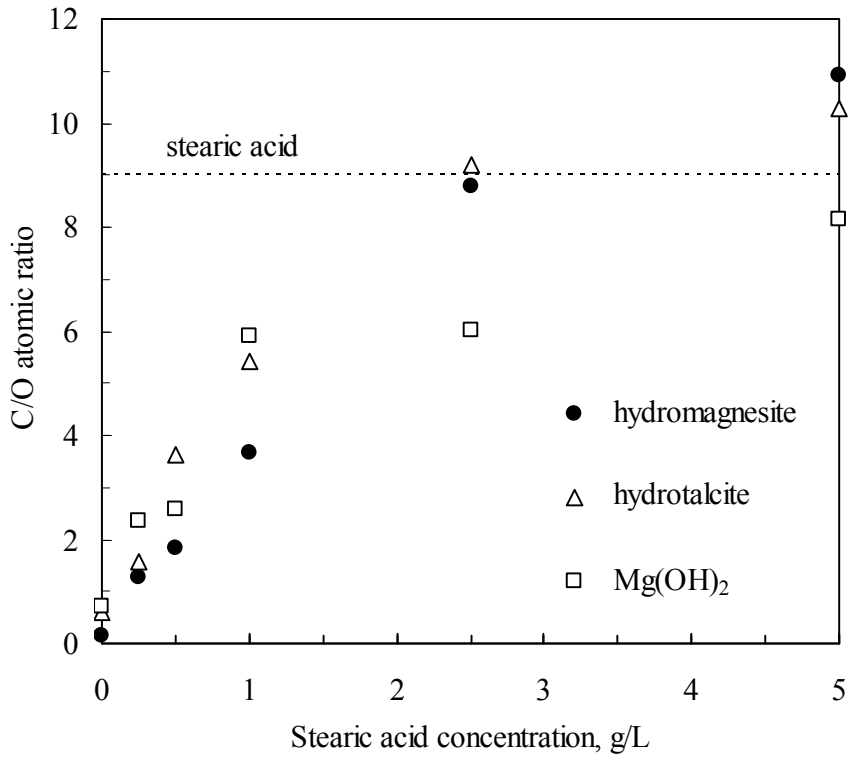

Figure 7. Effect of stearic acid dosage level on the C/O atomic ratio as estimated from XPS.

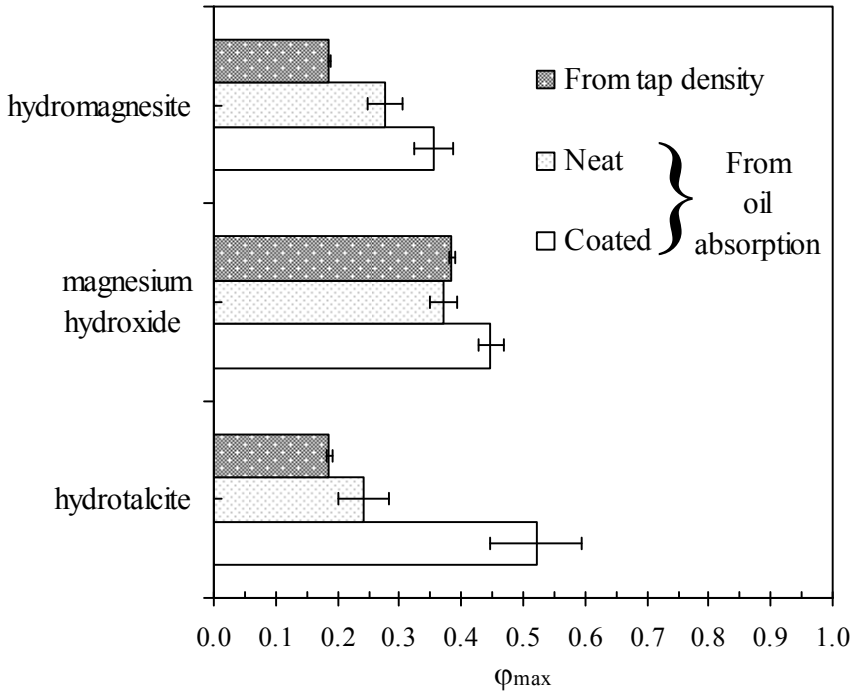

Figure 8. Specific maximum filler volume fractions determined from tap density (for uncoated filler only) and oil absorption experiments (uncoated and treated with 2.5 g/L stearic acid).

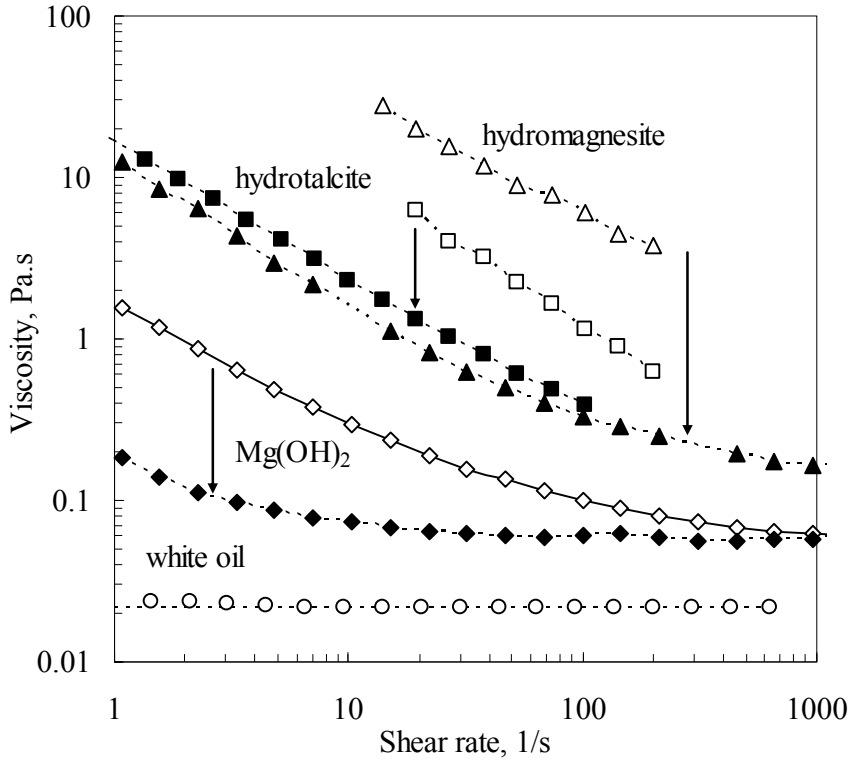

Figure 9. Effect of stearic acid coating on the viscosity of 25 wt % suspensions of hydromagnesite, magnesium hydroxide and hydrotalcite powders in white oil at 30 °C. Open symbols indicate neat powders while solid symbols are for powders treated with 2.5 g/L stearic acid solution in acetone. The arrows indicate the reduction in apparent viscosity facilitated by the surface coatings.